Communications on Applied Nonlinear Analysis
ISSN: 1074-133X
Vol 32 No. 2s (2025)

Nonlinear Improved Adaptive Optimized Grey Model for Real-Time Monitoring and Control of Weld Bead Geometry in Robot-Assisted Wire Arc Additive Manufacturing

Satish Kumar Parimi[1*], L Suvarna Raju [1,2], G. Mallaiah[3]

[1]Department of Mechanical Engineering, Vignan's Foundation for Science, Technology and Research, Andhra Pradesh, India

[2]Department of Mechanical Engineering Education, National Institute of Technical Teachers Training & Research (NITTTR), Bhopal, India

[3]Department of Mechanical Engineering, KITS, Singapur, Huzurabad.

Corresponding author*: satishniyogi1972@gmail.com

Article History:

Received: *19-09-2024*

Revised: *27-10-2024*

Accepted: *07-11-2024*

Abstract:

WAAM with directed energy deposition process and live monitoring of weld bead shape gives researchers and manufacturers real-time information, allowing them to regulate the metal deposition process layer by layer effectively. This work created an improved adaptive optimized grey model (IAOGM), for online monitoring of metal deposits' height and depth in each layer. The IAOGM(1,N) model takes fewer training samples and has limited information. To improve prediction accuracy, the training data was constantly updated by eliminating old data and introducing newer data. The framework's parameters comprised welding time, current, the absolute difference in current at 5-second intervals, and arc force. The best accurate weld bead height and depth estimates were obtained by calculating the root mean square error (RMSE) for various parameter combinations. The interplay of time, current, and arc force was discovered to have a considerable impact on weld bead diameters. Using these parameters, the model predicted weld bead height and depth with MAPE, RMSE, and MAE, values of 5.48, 3.32, and 7.56 respectively, when compared to experimental data. This technique enables users to properly balance process parameters and achieve desired weld bead heights without the requirement for substantial training.

Keywords: WAAM, Non-linear data model**,** Improved adaptive optimized grey model, Weld bead characteristics, Online monitoring

1. Introduction:

The advancement of Industry 5.0 transforms the conventional additive manufacturing(AM) methods with the use of robots and AI-based smart machines with or without the intervention of human beings to enhance sustainability. Technologies such as IoT-enabled smart machines and big data analytics are in industry 4.0 transformed into Robot-assisted AI-based smart machines with human-computer interaction (HCI) in concern with sustainability aspects. Additive manufacturing is attracting industry and researchers' attention globally due to its progressive and potential benefits[1]. As per the survey of the global additive market CAGR (Compound Annual Growth Rate) will be 22% in the next 5 years. The current USD 14.5 billion valued Additive manufacturing market will be projected to be USD 69 billion by 2030. Material versatility is one of the concerns of AM technologies to be addressed and studied further, especially with metal additive manufacturing. Due to excellent material utilization,

ease of flexibility, and its potential with high deposition it to be used in a vast range of applications such as automotive, textile, medical, jewelry, customized appliances, and even the most expensive aerospace industry because of its less buy-to-fly(BTF) ratio.[2] AM more often referred as 3D printing with metal as filament can be treated as metal additive manufacturing(MAM). The production across the industries are revolutionizing with MAM technologies. Among the MAM technologies, Direct energy deposition(DED) is renowned for its efficient material deposition. In the recent times, the ease of AM is gaining attention of researchers along with the industries. The complex intricate shapes are developed by process of material deposition as layer by layer[3]. Wire plus arc additive manufacturing(WAAM) adopts DED technology because of the advent features such as, ease of operation, and increased productivity with efficient material deposition which grasp the attention of researchers[4]. Using robots in manufacturing will enhance productivity with precision in performing works such as the robotic gas metal arc welding process(GMAW) which is based on DED technology with high potential beneficial aspects along with the automation. The dimensional accuracy of the deposited weld bead profiles is also an important concern, resulting in poor build structure of the weld bead. Surface quality is another barrier to the wide adoption of WAAM in all manufacturing sectors, affecting the building structure with voids and defects [5]. Further proper selection of process parameters is essential to obtain the homogeneous structure of the thin wall geometry produced by the WAAM process[6]. Before the selection of optimal process parameters researchers have to take a call on the modeling techniques available such as physics-driven models and data-driven models to control and monitor weld bead profiles. Most physics-driven models are based on the finite element method(FEM) based and data-driven models rely on the previous experimental history of the weld bead deposition in the formation of structures. As the FEM is derived from physics-driven modeling it requires a lot of computational effort and time along with the complex analytical equations. Hence data-driven models are preferable for convenient usage along with the control and monitoring of the weld bead profiles with enhanced surface quality and build structure integrity.

Data-driven models are considered as prominent alternatives to model the weld bead profile using the general-additive-model method to predict the weld bead dimensional characteristics[5]. The weld bead's dimensional characteristics along with the structural integrity and quality of the weld bead are significantly influenced by the input process parameters of the equipment most of the GMAW processes are combined with a Degree of freedom robot to automate the process and the parameters are weld speed, feed rate, input voltage for the process, with the equal significance of time for cooling in between weld beads or layers[7]. The effect of inter-pass temperature will affect the grain size in the microstructure of the weld bead which affects the mechanical performance parameters of the structure[8]. In few studies, it was identified that the multilayer weld bead deposition enhances the energy deposition which implies that deposition happens with a certain quantum of arc force which further leads to an increase in depth penetration of the weld bead[9]. The homogeneous weld bead formation will depend on the fine-tuning of process parameter selection, few researchers have identified that weld bead irregular formation at the starting and at the end of the bead is a generic problem with the WAAM and attention is required to control this phenomenon. Even though this critical issue is complex, it has been addressed by a geometrical leveling strategy by depositing an additional run of weld bead to compensate for the irregularities which consumes additional time to complete[10]. The uniformity of the weld bead is monitored with a passive vision system which is

integrated with PID controller to monitor and control the formation based on the feedback obtained from the most recently deposited weld bead [11]. In most situations, the innovative model has the highest forecasting precision, indicating that optimizing the beginning condition and background value may significantly improve the gray model's flexibility and prediction accuracy[12].From the literature, it is summarized that few researchers have reported limited number of studies on modeling methods for the estimation of wall structure geometry in WAAM process. But, the quality of the deposited structure and dimensional accuracy depends on the qualitative deposition of molten metal with appropriate arc force, hence the monitoring of weld bead deposition requires much attention. Hence, in the present study, in-process monitoring of weld bead deposition using novel robust in-process online grey forecasting model(OGM) frame work is adopted to monitor the weld bead geometry, such as width of the weld bead (WWB), height of the weld bead(HWB)& depth of the weld bead(DWB) in formation of thin wall structure in wire arc additive manufacturing. The input process parameters such as deposition time, arc force and current are considered as independent variables. The output process parameters such as width, height, and depth of the weld bead are forecasted by OGM.

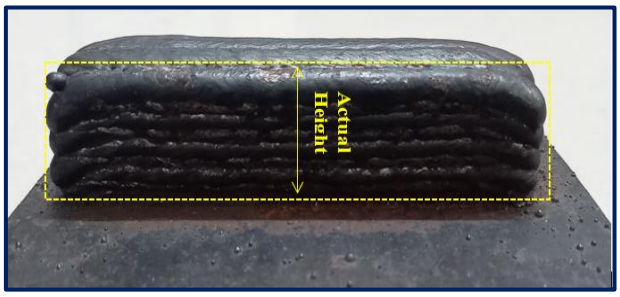

Fig.1 Wire arc additively manufactured Thin wall

1.1 Objective of the work:

In forming a thin wall structure formed by multiple weld beads layer by layer, the dimensional characteristics such as HWB, WWB, and DWB are dependent on process parameters used for the deposition of weld beads. The formation of weld bead throughout the deposition is not uniform, and the same kind of structure can be observed in the literature also, as the extreme positions of the weld bead differ from the middle segments of it, and the same is reported in the literature as well[10]. In the formation of intricate shapes via the WAAM process the varying cross-sectional weld bead deposition is considered as typical and deposition of like-wise weld beads to develop thin walls with varied dimensions requires adaptive weld bead formation with optimal process parameters as mentioned[13]. Accordingly, the most influencing process parameters in Robotic WAAM are wire feed, weld speed, current, and torch angle are selected for the present work. In the present work, the torch angle is taken as 79 degrees, which is optimal as per the existing literature. The objective of the present work to develop a novel and robust online monitoring and control system for weld bead dimensional characteristics with reduced MAPE value between forecasted and experimental results. So, the accuracy of the proposed model should be improved. In addition, a comparative study is to be made between the normal thin wall structure and the application of the proposed framework model.

1.2. Factors affecting the weld bead:

The parameters such as width and depth of weld beads are influenced by the mode of metal transfer, and its associated arc force[14]. The arc force in the metal transfer is a composition of forces from an electrode to the substrate is explained in this section.

The mode of metal transition from the filler wire to the substrate consists of a composition of forces which are described in different theories explained[15]. The static force theory focuses on the detaching phenomenon of metal drop-in metal transfer mode, when the metal drop retaining force is less than the static detaching force, the metal drop detaches from the electrode and sticks on the substrate[16]. This theory also states that metal drop detaching is under the association of gravity force, the current-produced electromagnetic force and plasma arc drag force while retaining force under the surface tension of the molten metal drop[17].

The gravity force of the metal drop is due to self-weight, which inhibits the ability to detach from feed wire and it is calibrated by the equation (1) and calculated as 3.55 × 10-3 N. As the molten filler metal drop transition is dependent on the arc current and the flow of metal drops is less, the globular mode of metal transfer occurs, and its volume (v) is under gravitational force. The diameter of a droplet is twice of the mild steel filler wire supplied, with the density (ρ_D) and force of gravity (g) taken as 0.00785 gmm-3 and 7.83 gmm-3 respectively[18]. In the present work the experiments are performed with conventional industry power ratings and process parameters are selected [19].

$$P_g = v\,\rho_D\,g \qquad (1)$$

The electromagnetic force associated is determined[18] by equation (2)

$$P_{emf} = \frac{CI^2}{4\pi}\mu_0 \qquad (2)$$

Magnetic permeability (μ_0) in the calibration of the electromagnetic force is

considered as 12.57 × 10-7 NA-2. The coefficient of globular mode

arc is treated as 1 Jones et al as for the molten metal droplet[18]. The plasma arc drag force on the metal droplet is described by equation (3)

$$P_p = \frac{\pi}{2}(R^2 - r^2)\,C_d v_p^2 \rho_p \qquad (3)$$

The plasma drag constant (C_d) is 0.44 and it is calculated as 5.11 × 10-3 N, where v_p is the speed rate and ρ_p is the density of the droplet of radius R[20].

The net arc force (PA) required to exceed molten metal drop retaining force and to detach from the tip of the nozzle to the substrate is given by equation (4)

$$P_A = P_g + P_{emf} + P_p \qquad (4)$$

1.3 Discrete Grey Forecasting Model:

The grey system theory was proposed by the renowned professor Deng, to predict the future data effectively from the small portions of existing data. Classical grey modeling techniques are widely used in parameter estimation and structural optimization[12][21]. Initially, the GM (1,1) model is only

applicable to exponential series data. Later, researchers increased the model's flexibility to deal with nonlinear data[22]. In addition, an adaptive and optimized grey Bernoulli model was presented to cope with restricted time series data containing stochastic disturbance. To address the time delay effect, a time-delayed and power-driven (GMTDPD) grey model is presented, as well as an improved adaptive optimized grey model (IAOGM) for prediction models containing nonlinear, changing data sequences. The randomness of the raw time data series will vanish after performing accumulated generation operations repeatedly.

Usually, Grey forecasting models utilize the limited data sets in 0^{th} order as indicated as DGM(0,N), where 0 represents the order of accumulation and N represents the number of variables (both dependent and independent). The first order accumulated generation operation (I-AGO) is indicated as DGM(1,N)[23]. In general the Discreete grey forecasting model is shown as follows[24]:

$$\{X_i^{(0)}\} = \{X_i^{(0)}(1), X_i^{(0)}(2), X_i^{(0)}(3), \ldots\ldots, X_i^{(0)}(n)\} \quad (5)$$

Where n represents the number of data samples in the sequence, and $X_i^{(0)}$ is the number of the variable sequences.

As per the definition of grey prediction model the I-AGO series of $X_i^{(0)}$ is given by ():

$$\{X_i^{(1)}\} = \{X_i^{(1)}(1), X_i^{(1)}(2), X_i^{(1)}(3), \ldots\ldots, X_i^{(1)}(n)\} \quad (6)$$

In DGM(1,N), if N=4, the grey forecasting model consists of single dependent variable and three independent variables. The sequence of the data variables are given as:

Sequence of the data variable -1: $\{X_1^{(1)}\} = \{X_1^{(1)}(1), X_1^{(1)}(2), X_1^{(1)}(3), \ldots\ldots, X_1^{(1)}(n)\}$ (7)

Sequence of the data variable -2: $\{X_2^{(1)}\} = \{X_2^{(1)}(1), X_2^{(1)}(2), X_2^{(1)}(3), \ldots\ldots, X_2^{(1)}(n)\}$ (8)

Sequence of the data variable -3: $\{X_3^{(1)}\} = \{X_3^{(1)}(1), X_3^{(1)}(2), X_3^{(1)}(3), \ldots\ldots, X_3^{(1)}(n)\}$ (9)

Sequence of the data variable -4: $\{X_4^{(1)}\} = \{X_4^{(1)}(1), X_4^{(1)}(2), X_4^{(1)}(3), \ldots\ldots, X_4^{(1)}(n)\}$ (10)

Where $\{X_m^1(p)\} = \sum_{n-1}^{p} X_m^{(0)}(n), p = 1,2,3, \ldots\ldots, q$

The mean of the sequence, generated from $X_m^1(p)$, now

$\{Z_m^{(1)}\} = \{Z_m^{(1)}(2), Z_m^{(1)}(3), Z_m^{(1)}(4), \ldots\ldots, Z_m^{(1)}(n)\}$ if N= 4, then m=1,2,3 &4

Where

$Z_m^{(1)}(p) = \frac{X_m^1(p-1)+X_m^1(p)}{2}, p = 2,3,4, \ldots q$, then the model DGM (1, N) is given as:

$X_m^1(p) + aZ_m^{(1)}(p) = \sum_m^N X_m^{(1)}(p)$

Further, the least square method is used to estimate the sequence of the parameters of DGM (1, N) as follows:

$$\vec{a} = [a, b_1, b_2, \ldots\ldots, b_N]^T$$

Where a is the system coefficient and b terms are the driving coefficients of the model. It can be written as

$$\vec{a} = (B^T B)^{-1} B^T Y$$

Where the B matrix and Y matrix are estimated as

$$B=\begin{bmatrix} -z_1^{(1)}(2) & -z_2^{(1)}(2) & \cdots & -z_N^{(1)}(2) \\ -z_1^{(1)}(3) & -z_2^{(1)}(3) & \cdots & -z_N^{(1)}(3) \\ \cdots & \cdots & \cdots & \cdots \\ -z_1^{(1)}(m) & -z_2^{(1)}(m) & \ddots & -z_N^{(1)}(m) \end{bmatrix} \quad Y = \begin{bmatrix} X_1^{(0)}(2) \\ X_1^{(0)}(3) \\ \vdots \\ X_1^{(0)}(m) \end{bmatrix}$$

The robust grey forecasting models are the potential in forecasting the dependent parameters which is the response of the DGM (1, N) with the reduced MAPE(). The Model is estimated as:

$$X_1^{(0)}(k) + az_1^{(1)}(m) = \sum_{i=2}^{N} b_i X_i^{(1)}(k) + h_1(k-1) + h_2$$

Where h_1, h_2 *are linear corrections of the grey model*. The parameter sequence of the Predicting model with the coefficient $\vec{r}$ is described as:

$$\vec{r} = [a, b_1, b_2, b_3, \ldots., b_N, \quad h_1, h_2]^T$$

$$\vec{r} = (B^T B)^{-1} B^T Y$$

Where

$$B = \begin{bmatrix} X_1^{(1)}(2) & X_2^{(1)}(2) & \cdots & X_N^{(1)}(2) & -z_1^{(1)}(2) & 1 & 1 \\ X_1^{(1)}(3) & X_2^{(1)}(3) & \cdots & X_N^{(1)}(3) & -z_1^{(1)}(3) & 2 & 1 \\ \vdots & \vdots & \vdots & \vdots & \vdots & \vdots & 1 \\ X_1^{(1)}(m) & X_2^{(1)}(m) & \ddots & X_N^{(1)}(m) & -z_1^{(1)}(m) & m-1 & 1 \end{bmatrix} \quad Y = \begin{bmatrix} X_1^{(0)}(2) \\ X_1^{(0)}(3) \\ \vdots \\ X_1^{(0)}(m) \end{bmatrix}$$

The output response of the IOGM (1, N) model is estimated by the equation mention below:

$$\breve{X}_1^{(0)}(k) = \mu_1 \sum_{i=2}^{N} b_i X_i^{(1)}(k) + \mu_2 \breve{X}_1^{(1)}(k-1) + \mu_3 k + \mu_4, \mathrm{k} = 2,3,4, \ldots \mathrm{n}$$

Where $\mu_1 = (1 + 0.5a)^{-1}$

$$\mu_2 = (1 + 0.5a)^{-1}$$

$$\mu_3 = h_1(1 + 0.5a)(1 + 0.5a)^{-1}$$

$$\mu_4 = (h_2 - h_1)(1 + 0.5a)^{-1}$$

Accordingly, HWB, DWB, WWB responses are estimated using the above equation.

The GM (1,1) model is frequently employed for analysis of time series due to its ability to adapt to uncertain systems with little data. information. This section will discuss the concepts and faults of the original GM (1,1) model. The IAOGM (1,1) model is proposed to address the primary error causes of GM (1,1), which are based on the starting and background values. This IAOGM (1,1) model's precise techniques for coordinating two optimum approaches will be investigated and analysed.

The IAOGM (1,1) model improves two elements based on the intrinsic error sources of the GM (1,1) model, as discussed in Section 3.1. On the one hand, with the intention to gain a Preliminary Condition After considering all observations and prioritizing the most recent information, a new weighted series is used to create a modified starting condition that aligns with the evolving system. Simpson's formula is used to construct the background value, which is crucial for enhancing the grey model's applicability to high-growth exponential sequences. It addresses integral issues. Simpson's formula is used in sequences to provide background values that can manage integral difficulties. The IAOGM (1,1) model's processes are outlined in the stages below, leveraging its superiority. Figure 2 illustrates the summary flowchart for the IAOGM (1,1) model.

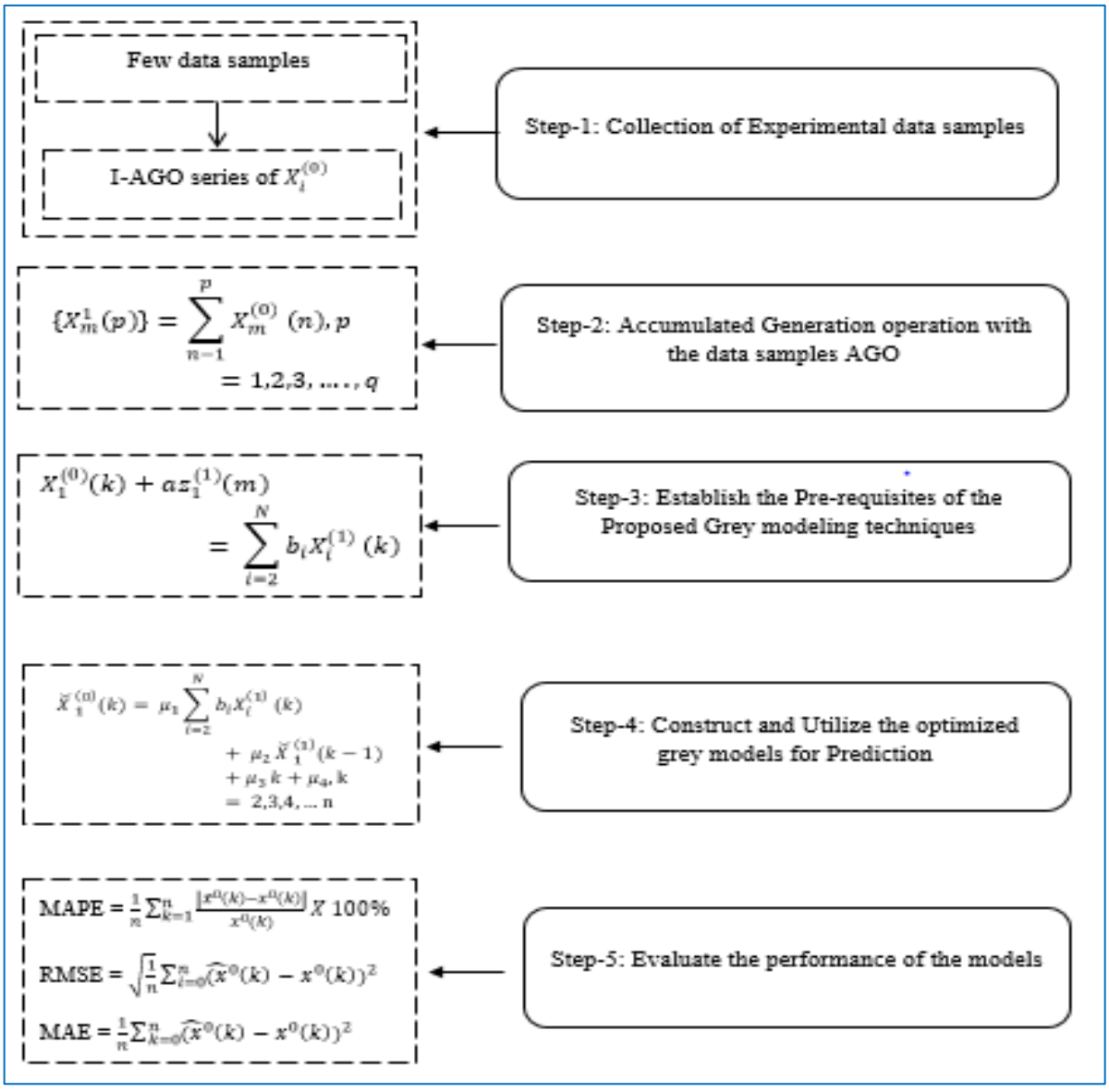

The improved adaptive optimized grey model IAOGM:

2. Experimentation:

In the present work, experimentation was carried out using an industrial-grade IRB 1520 MIG robot as shown in the Fig.2. Robot-assisted wire arc additive manufacturing used as an alternative to metal additive manufacturing due to the ease of operation and most resourceful, instead of expensive metal 3D printers in the market. As the equipment of industry-standard, industrial power rating was used in the work to study the deposition of weld beads as layers. The controller is equipped with a teach pendant, an instrument to work with the robot. The geometrical motions involved in the deposition of the weld beads to form the structure are customized and pre-programmed using rapid code. As shown in the figure a metal substrate of customized size as per the structure to be formed, is rigidly clamped to the fixed platform of the robot. The operating requirements of the robot such as voltage, weld feed speed, weld speed, and shielding gas supply are taken as 18V, 4 m/min, 0.3 m/min and 20 l/min. The filler wire of 1.2 mm diameter of AISI 1018 steel material is used. AISI 1018 steel is widely used in industries due to its ability to uniform weld beads and also offers superior machining characteristics with excellent weldability properties.

Fig.2 IRB 1520 Robot cell

The experiment was performed in two phases. In the first phase, the substrate was rigidly fixed as shown in the figure with the help of clamps as also simulated in the simulation. The weld beads were on the substrate with the help of a robot as shown in Fig.1. At every 4-second instance during the weld bead formation the current was measured with the help of a kempi arc controller. The average feed rate is also measured along with the current. After the formation of the initial layer, the weld bead was sectioned at 5 different locations with the wire EDM, and the corresponding weld bead characteristics were measured using stereo zoom microscopy. From the first phase, it was observed different weld bead characteristics such as height, width, and depth. In the later phase, weld beads were deposited on the substrate using a multi-bead formation strategy with a time halt of 5 seconds among the layup of 12 fully overlapped multi-weld beads. Similarly, the dimensions were measured at 5 locations as measured in the 1st phase. The measured features at 5 locations are tabulated.

Table 1. Weld bead dimensional features at 5 different locations

S. No.	Weld Bead No. (n)	T (min)	I (A)	ΔI (A)	AFX 10^-3 (N)	DWB (mm)	WWB (mm)	HWBi (mm)	HWBi	Total HWB
1	1	5	190.5	0	12.35	1.28	3.81	2.7	0	2.7
2	1	10	174.2	16.3	11.71	1.03	3.06	3.43	0	3.43
3	1	15	180.8	6.6	11.95	1.34	3.99	3.05	0	3.05
4	1	20	186.4	5.6	12.15	1.52	4.53	2.53	0	2.53
5	1	25	191.9	5.5	12.36	1.75	5.22	2.72	0	2.72
6	1	30	197.3	5.4	12.57	1.98	5.91	2.35	0	2.35
7	2	35	191.5	5.8	12.35	1.3	3.87	3.02	2.7	5.72
8	2	40	175.4	16.1	11.76	1.06	3.15	2.75	3.43	6.18
9	2	45	179.9	4.5	11.92	1.32	3.93	2.66	3.05	5.71
10	2	50	186	6.1	12.14	1.55	4.62	2.7	2.53	5.23
11	2	55	193.2	7.2	12.41	1.76	5.25	1.98	2.72	4.7
12	2	60	198.3	5.1	12.61	2.01	6	2.02	2.35	4.37
13	3	65	191.2	7.1	12.34	1.33	3.96	2.31	5.4	7.71
14	3	70	173	18.2	11.67	1.1	3.27	3.29	6.86	10.15
15	3	75	183.2	10.2	12.04	1.31	3.9	3.22	6.1	9.32
16	3	80	185.8	2.6	12.13	1.54	4.59	2.02	5.06	7.08
17	3	85	194.1	8.3	12.15	1.8	5.37	2.83	5.44	8.27
18	3	90	198.6	4.5	12.14	2.03	6.06	2.06	4.7	6.76
19	4	95	192	6.6	12.17	1.32	3.93	3.88	9.28	13.16
20	4	100	173.7	18.3	12.18	1.13	3.36	3.03	9.89	12.92
21	4	105	184.1	10.4	12.18	1.34	3.99	2.97	9.07	12.04
22	4	110	185.3	1.2	12.17	1.62	4.83	3.13	8.19	11.32
23	4	115	192.4	7.1	12.15	1.82	5.43	2.19	7.63	9.82
24	4	120	196.5	4.1	12.14	2.14	6.39	2.14	6.84	8.98
25	5	125	188.8	7.7	12.16	1.4	4.17	1.78	5.28	7.06
26	5	130	172.7	16.1	12.17	1.14	3.39	3.2	4.17	7.37
27	5	135	182.3	9.6	12.18	1.4	4.17	2.78	4.37	7.15
28	5	140	188	5.7	12.16	1.61	4.8	3.35	4.74	8.09
29	5	145	191.7	3.7	12.13	1.82	5.43	2.92	4.01	6.93
30	5	150	197.5	5.8	12.12	2.14	6.39	3.15	4.28	7.43
31	6	155	191.2	6.3	12.15	1.38	4.11	2.91	3.16	6.07
32	6	160	175.4	15.8	12.16	1.14	3.39	3.03	8.31	11.34
33	6	165	181.6	6.2	12.16	1.4	4.17	2.42	6.59	9.01
34	6	170	187	5.4	12.16	1.65	4.92	1.39	5.76	7.15
35	6	175	192.8	5.8	12.16	1.83	5.46	1.63	6.37	8
36	6	180	195.6	2.8	12.16	2.15	6.42	2.16	6.17	8.33

37	7	185	193.1	2.5	12.16	1.44	4.29	2.52	5.68	8.2
38	7	190	173.3	19.8	12.15	1.18	3.51	2.63	10.94	13.57
39	7	195	183.7	10.4	12.15	1.43	4.26	2.63	9.22	11.85
40	7	200	185	1.3	12.15	1.67	4.98	2.91	8.67	11.58
41	7	205	193.8	8.8	12.15	1.83	5.46	3.51	9.88	13.39
42	7	210	196.4	2.6	12.15	2.15	6.42	2.02	8.19	10.21
43	8	215	189.5	6.9	12.15	1.5	4.47	2.92	8.6	11.52
44	8	220	176	13.5	12.15	1.18	3.51	4.37	15.31	19.68
45	8	225	179.7	3.7	12.15	1.41	4.2	2.65	11.87	14.52
46	8	230	187.3	7.6	12.15	1.67	4.98	3.23	11.9	15.13
47	8	235	194.2	6.9	12.15	1.84	5.49	1.75	11.63	13.38
48	8	240	199	4.8	12.15	2.16	6.45	1.11	9.3	10.41
49	9	245	192.1	6.9	12.15	1.55	4.62	3.47	12.07	15.54
50	9	250	171.4	20.7	12.15	1.22	3.63	3.1	18.41	21.51
51	9	255	181.9	10.5	12.15	1.47	4.38	2.94	14.81	17.75
52	9	260	184.5	2.6	12.15	1.72	5.13	1.91	13.81	15.72
53	9	265	194.7	10.2	12.15	1.86	5.55	2.85	14.48	17.33
54	9	270	198.4	3.7	12.15	2.16	6.45	3.41	12.71	16.12
55	10	275	190.5	7.9	12.15	1.58	4.71	2.33	14.4	16.73
56	10	280	174.2	16.3	12.15	1.22	3.63	2.64	21.05	23.69
57	10	285	180.8	6.6	12.15	1.51	4.5	3.22	18.03	21.25
58	10	290	186.4	5.6	12.15	1.73	5.16	3.16	16.97	20.13
59	10	295	192.1	5.7	12.15	1.88	5.61	2.43	16.91	19.34
60	10	300	197.3	5.2	12.15	2.16	6.45	2.07	14.78	16.85
61	11	305	184.5	12.8	12.15	1.78	5.31	3.47	17.87	21.34
62	11	310	194.7	10.2	12.15	1.24	3.69	3.1	24.15	27.25
63	11	315	198.4	3.7	12.15	1.53	4.56	2.94	20.97	23.91
64	11	320	190.5	7.9	12.15	1.74	5.19	1.91	18.88	20.79
65	11	325	174.2	16.3	12.15	1.89	5.64	2.85	19.76	22.61
66	11	330	180.8	6.6	12.15	2.34	6.99	3.41	18.19	21.6
67	12	335	186.4	5.6	12.15	1.8	5.37	2.33	20.2	22.53
68	12	340	192.1	5.7	12.15	1.26	3.75	2.64	26.79	29.43
69	12	345	197.3	5.2	12.15	1.55	4.62	3.22	24.19	27.41
70	12	350	189.5	7.8	12.15	1.76	5.25	3.16	22.04	25.2
71	12	355	176	13.5	12.15	1.91	5.7	2.43	22.19	24.62
72	12	360	179.7	3.7	12.15	2.36	6.82	2.07	20.26	22.33

2.1. Validation of the proposed model:

To accurately predict future trends, it's important to use proper testing criteria after estimating outcomes using competing models. As a result, the testing criteria should be able to detect the

discrepancy between real observations and estimated values. This article uses four statistical assessment indicators: Mean absolute percentage error (MAPE), and root mean squared error (RMSE), and mean absolute error (MAE), which are described below.

$$\text{MAPE} = \frac{1}{n}\sum_{k=1}^{n}\frac{|\hat{x}^0(k)-x^0(k)|}{x^0(k)} X\ 100\%$$

$$\text{RMSE} = \sqrt{\frac{1}{n}\sum_{i=0}^{n}\widehat{(x}^0(k) - x^0(k))^2}$$

$$\text{MAE} = \frac{1}{n}\sum_{k=0}^{n}\widehat{(x}^0(k) - x^0(k))^2$$

where the $x^{(0)}(k)$ is experimental value, and the $\hat{}x^{(0)}(k)$ is predicted value.

Low values for indicators indicate better predicting ability with greater precision. Table 2 shows the accuracy levels calculated using MAPE values.

3. Results and Discussions

3.1. Prediction of HWB, WWB, DWB

Fig.3 describes the temporal evolution of the measured parameter "HWB (mm)" for 12 distinct bead categories (BEAD-1 to BEAD-12) over 60 seconds. The measurements were recorded at 5-econd intervals. All bead categories exhibit a progressive increase in HWB values with time.

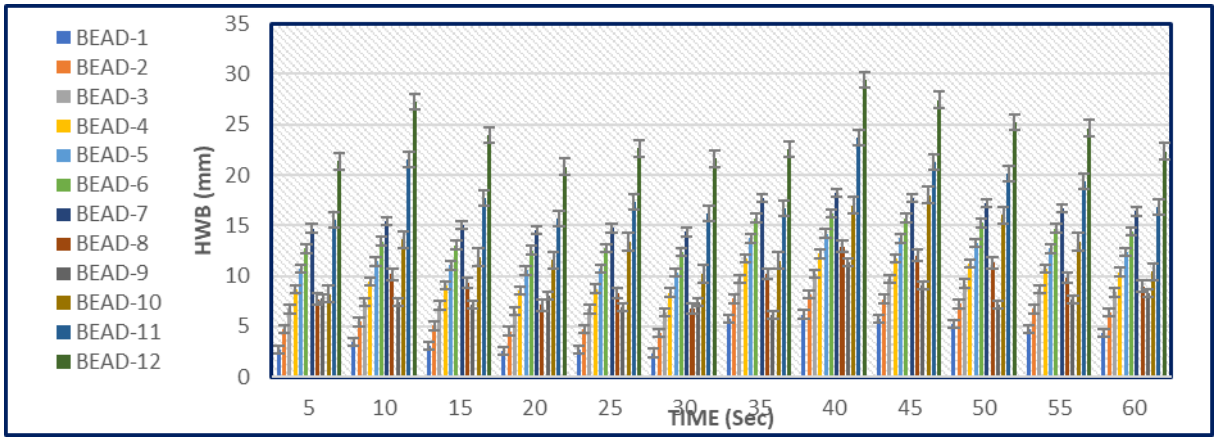

Fig.3. HWB for 12 distinct bead categories (BEAD-1 to BEAD-12) over a period of 60 Seconds.

This indicates a dynamic process influencing the bead characteristic, such as swelling, growth, or reaction to an external stimulus. BEAD-12 consistently shows the highest HWB values across all time points, suggesting either a unique composition or interaction compared to other bead types. Conversely, categories like BEAD-1 and BEAD-2 display the lowest HWB values, highlighting a significant disparity in behaviour or properties.

Fig.4, & Fig.5, reveal the temporal progression of "WWB (nm)" values for 12 bead categories (BEAD-1 to BEAD-12) measured at intervals of 5 seconds, spanning a total duration of 60 seconds. The WWB values for all bead categories exhibit a stepwise increase over time, indicating a consistent growth or change in the measured parameter across the 60-second duration. This could reflect a time-dependent process, such as swelling, absorption, or another reaction occurring in the beads. Although all beads

follow a similar overall trend, slight variations are observed among different bead categories: BEAD-12 and BEAD-6 appear to have the highest WWB values at each time interval. BEAD-1 and BEAD-2 show relatively lower WWB values compared to other groups, suggesting differing material properties or responses to the experimental conditions.

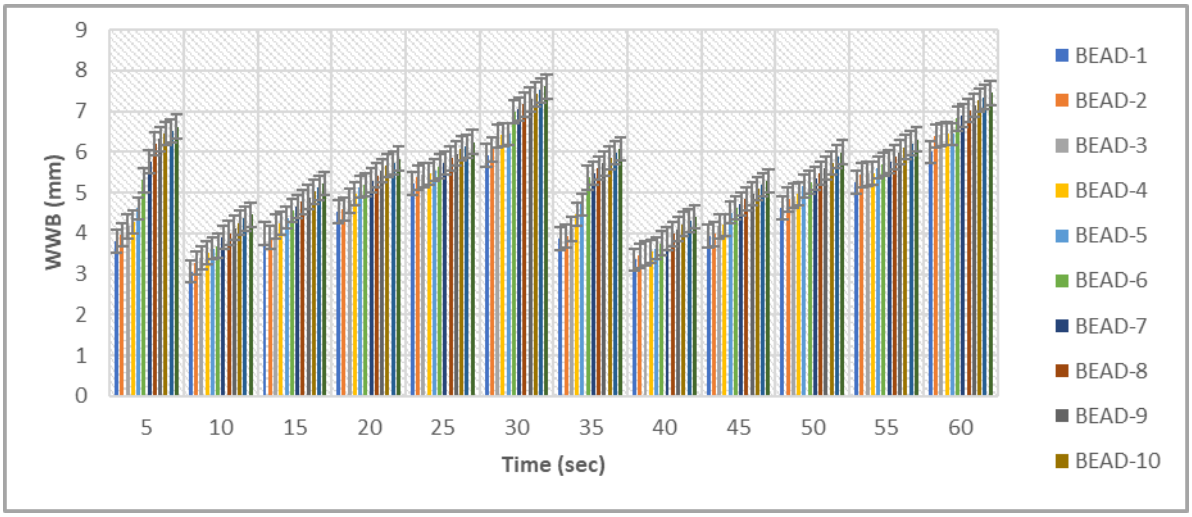

Fig.4. WWB for 12 distinct bead categories (BEAD-1 to BEAD-12) over a period of 60 Seconds.

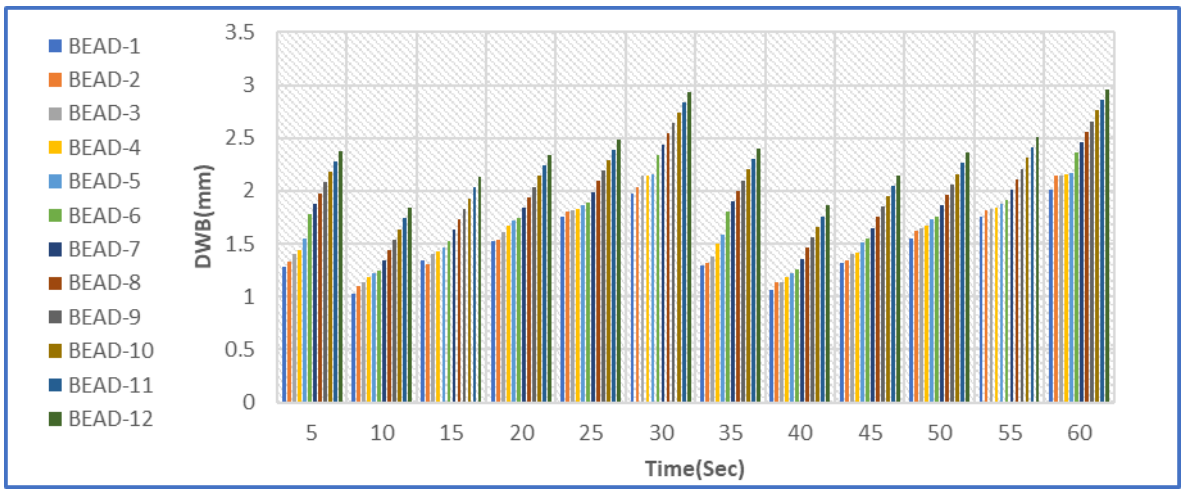

Fig.5. DWB for 12 distinct bead categories (BEAD-1 to BEAD-12) over a period of 60 Seconds.

Table.2 Experimental vs Predicted errors

Phase	Method	DGM(1,1)	OGM(1,1)	IAOGM (1,1)
Experimental	MAPE	5.65	4.36	3.85
	RMSE	12.45	11.5	12.72
	MAE	17.23	18.34	18.56
Predicted	MAPE	8.34	7.47	5.48
	RMSE	3.54	4.52	3.32
	MAE	6.45	5.74	7.56

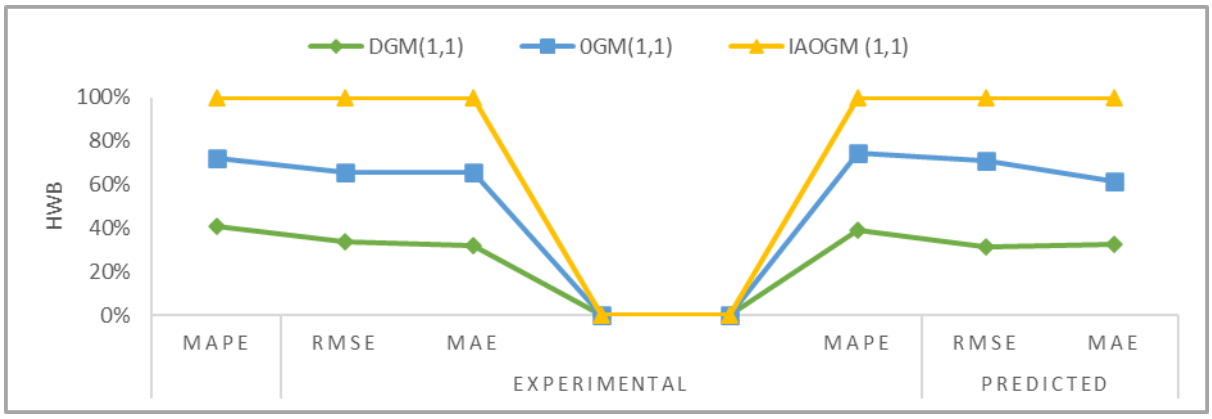

Fig.6. Comparison of experimental and predicted methods

DGM (1,1), OGM (1,1), and IAOGM (1,1)—using different error metrics across experimental and predicted phases. In the experimental phase, IAOGM (1,1) outperforms the other methods in terms of Mean Absolute Percentage Error (MAPE) with the lowest value of 3.85, indicating higher accuracy. However, OGM (1,1) shows the lowest Root Mean Square Error (RMSE) at 11.5, suggesting slightly better error consistency compared to the others, whereas DGM (1,1) achieves the lowest Mean Absolute Error (MAE) at 17.23. For the predicted phase, IAOGM (1,1) again demonstrates superior performance with the lowest MAPE (5.48) and RMSE (3.32), highlighting its robust forecasting ability. However, OGM (1,1) yields the lowest MAE (5.74) in this phase, slightly edging out the other methods in absolute error terms. Overall, IAOGM (1,1) shows a balance of high accuracy and error consistency across both phases, making it the most reliable method among the three as shown in Fig.6

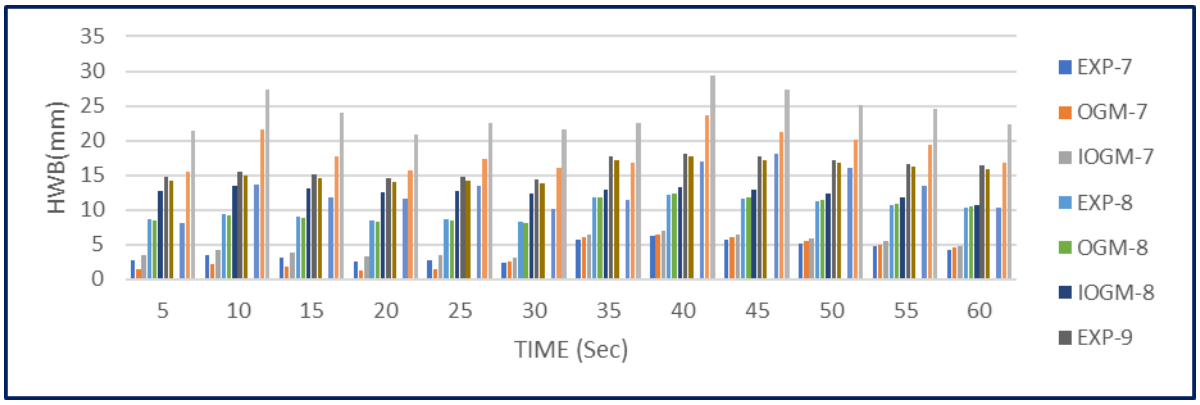

Fig. 7. HWB prediction using IAOGM

The proposed IAOGM (1, N) model successfully monitors the height of the weld beads as show shown in Fig.7 that deposits as layer by layer, utilizing real-time data to improve accuracy.

4. Conclusions:

This study demonstrates the effectiveness of an Improved Adaptive Optimized Grey Model (IAOGM) for real-time monitoring and prediction of weld bead shape in the WAAM (Wire Arc Additive Manufacturing) process using directed energy deposition. From the study, the following conclusions have been derived.

1. The developed IAOGM (1, N) model successfully monitored the height and depth of metal deposits layer by layer, leveraging real-time data updates to improve prediction accuracy. Experimental results validated the model's ability to provide reliable predictions, with the best performance achieved in the predicted phase, where MAPE, RMSE, and MAE values were 5.48, 3.32, and 7.56, respectively, demonstrating superior accuracy compared to other forecasting methods like DGM (1,1) and OGM (1,1).
2. The analysis of the provided graphs further substantiates these findings. The WWB (nm) and HWB (nm) trends highlighted the temporal changes in weld bead parameters, illustrating how process conditions such as time, current, and arc force significantly influence bead dimensions.
3. The IAOGM (1, N)'s ability to incorporate these factors into its predictive framework allowed for precise estimation of weld bead characteristics, as demonstrated by the low error margins observed across all metrics.
4. The integration of this model with WAAM processes enables manufacturers to effectively regulate metal deposition in real time, reducing reliance on extensive training data and manual intervention. This approach not only ensures optimal weld bead quality but also provides a scalable solution for future applications in additive manufacturing, where precision and adaptability are critical.
5. By continually updating training data and considering parameter interdependencies, the IAOGM (1, N) framework presents a significant advancement in achieving desired weld bead dimensions, paving the way for more efficient and reliable WAAM processes.

References

[1] P. K. R. Maddikunta *et al.*, "Industry 5.0: A survey on enabling technologies and potential applications," *J. Ind. Inf. Integr.*, vol. 26, no. February, p. 100257, 2022, doi: 10.1016/j.jii.2021.100257.
[2] O. İyibilgin and E. Gepek, "Additive Manufacturing Technologies and its Future in Industrial Applications," *Int. J. Integr. Eng.*, vol. 13, no. 5, pp. 245–257, 2021, doi: 10.30880/ijie.2021.13.07.028.
[3] K. C. Ying, F. Fruggiero, P. Pourhejazy, and B. Y. Lee, "Adjusted Iterated Greedy for the optimization of additive manufacturing scheduling problems," *Expert Syst. Appl.*, vol. 198, p. 116908, Jul. 2022, doi: 10.1016/J.ESWA.2022.116908.
[4] B. Panda, K. S. Akhil, and G. M. M. Savalani, "Evaluation of genetic programming-based models for simulating bead dimensions in wire and arc additive manufacturing," *J. Intell. Manuf.*, vol. 30, no. 2, pp. 809–820, 2019, doi: 10.1007/s10845-016-1282-2.
[5] C. Ruiz, D. Jafari, V. V. Subramanian, T. H. J. Vaneker, W. Ya, and Q. Huang, "Prediction and Control of Product Shape Quality for Wire and Arc Additive Manufacturing," vol. 144, no. November, pp. 1–11, 2022, doi: 10.1115/1.4054721.
[6] K. Drosos and S. Kotsakis, "Influence of welding parameters on weld quality and productivity using metal cored wires," *Dep. Mater. Manuf. Technol. Chalmers Univ. Technol. Gothenburg, Sweden*, pp. 1–60, 2014.
[7] M. Dinovitzer, X. Chen, J. Laliberte, X. Huang, and H. Frei, "Effect of Wire and Arc Additive Manufacturing (WAAM) Process Parameters on Bead Geometry and Microstructure," no. May, 2019, doi: 10.1016/j.addma.2018.12.013.
[8] B. Parvaresh, R. Miresmaeili, and M. Yazdizadeh, "Characterization of wire arc additive manufactured products: A comparison between as-deposited and inter-layer cold worked specimens," *J. Manuf. Process.*, vol. 57, no. June, pp. 61–71, 2020, doi: 10.1016/j.jmapro.2020.05.053.
[9] E. Aldalur, F. Veiga, A. Suárez, J. Bilbao, and A. Lamikiz, "Analysis of the wall geometry with different strategies for high deposition wire arc additive manufacturing of mild steel," *Metals (Basel).*, vol. 10, no. 7, pp. 1–19, 2020, doi: 10.3390/met10070892.
[10] Z. Wang and G. Abba, "Improvement strategy for the geometric accuracy of bead ' s beginning and end parts in wire-arc additive manufacturing (WAAM)," pp. 2139–2151, 2022.

[11] J. Xiong, Y. Zhang, and Y. Pi, "Control of deposition height in WAAM using visual inspection of previous and current layers," *J. Intell. Manuf.*, vol. 32, no. 8, pp. 2209–2217, 2021, doi: 10.1007/s10845-020-01634-6.

[12] S. Ding and R. Li, "Engineering Applications of Artificial Intelligence Forecasting the sales and stock of electric vehicles using a novel self-adaptive optimized grey model," *Eng. Appl. Artif. Intell.*, vol. 100, no. January, p. 104148, 2021, doi: 10.1016/j.engappai.2020.104148.

[13] B. K. R. Kunchala, S. Gamini, and T. C. Anilkumar, "Inclusion of IoT technology in additive manufacturing: Machine learning-based adaptive bead modeling and path planning for sustainable wire arc additive manufacturing and process optimization," *Proc. Inst. Mech. Eng. Part C J. Mech. Eng. Sci.*, vol. 237, no. 1, 2023, doi: 10.1177/09544062221117660.

[14] S. Krishnaveni, B. R. Kunchala, S. Gamini, and T. Ch Anilkumar, "Machine learning-based bead modeling of wire arc additive manufacturing (WAAM) using an industrial robot," *Mater. Today Proc.*, no. xxxx, 2023, doi: 10.1016/j.matpr.2023.04.534.

[15] R. Israr, J. Buhl, and M. Bambach, "A study on power-controlled wire-arc additive manufacturing using a data-driven surrogate model," *Int. J. Adv. Manuf. Technol.*, vol. 117, no. 7–8, pp. 2133–2147, 2021, doi: 10.1007/s00170-021-07358-y.

[16] M. Guo, C. Jia, J. Zhou, W. Liu, and C. Wu, "Investigating the generation process of molten droplets and arc plasma in the confined space during compulsively constricted WAAM," *J. Mater. Process. Technol.*, vol. 275, no. August 2019, p. 116355, 2020, doi: 10.1016/j.jmatprotec.2019.116355.

[17] L. A. Jones, T. W. Eagar, and J. H. Lang, "Magnetic forces acting on molten drops in gas metal arc welding," *J. Phys. D. Appl. Phys.*, vol. 31, no. 1, pp. 93–106, 1998, doi: 10.1088/0022-3727/31/1/013.

[18] Y. S. K. T.W.Eagar, "Analysis of metal transfer in gas metal arc welding," *Weld. Res. Suppl.*, vol. Weld. J. 7, doi: 10.1063/1.5114003.

[19] A. Busachi, J. Erkoyuncu, P. Colegrove, F. Martina, and J. Ding, "Designing a WAAM based manufacturing system for defence applications," *Procedia CIRP*, vol. 37, no. 2013, pp. 48–53, 2015, doi: 10.1016/j.procir.2015.08.085.

[20] T. Feucht, J. Lange, M. Erven, C. B. Costanzi, U. Knaack, and B. Waldschmitt, "Additive manufacturing by means of parametric robot programming," *Constr. Robot.*, vol. 4, no. 1–2, pp. 31–48, 2020, doi: 10.1007/s41693-020-00033-w.

[21] S. Ding, R. Li, S. Wu, and W. Zhou, "Application of a novel structure-adaptative grey model with adjustable time power item for nuclear energy consumption forecasting," *Appl. Energy*, vol. 298, p. 117114, Sep. 2021, doi: 10.1016/J.APENERGY.2021.117114.

[22] K. B. Reddy, G. Suresh, R. K. Mandava, and T. C. Anil Kumar, *A Short Review on Biped Robots Motion Planning and Trajectory Design*. 2022. doi: 10.1007/978-981-16-8341-1_39.

[23] M. Xia and W. K. Wong, "A seasonal discrete grey forecasting model for fashion retailing," *Knowledge-Based Syst.*, vol. 57, pp. 119–126, 2014, doi: 10.1016/j.knosys.2013.12.014.

[24] B. Wei, N. Xie, and Y. Yang, "Data-based structure selection for unified discrete grey prediction model," *Expert Syst. Appl.*, vol. 136, pp. 264–275, 2019, doi: 10.1016/j.eswa.2019.06.053.